THE ASTROPHYSICAL JOURNAL, 477:568–573, 1997 March 10

THE DUST-TO-GAS RATIO IN THE DAMPED Lyα CLOUDS TOWARD THE GRAVITATIONALLY LENSED QSO 0957+561

LIN ZUO, E. A. BEAVER, E. MARGARET BURBIDGE, ROSS D. COHEN, VESA T. JUNKKARINEN, AND R. W. LYONS
Center for Astrophysics and Space Sciences 0424, University of California, San Diego, La Jolla, CA 92093-0424
Received 1996 June 20; accepted 1996 September 25

ABSTRACT

We present *HST*/FOS[1] spectra of the two bright images (A and B) of the gravitationally lensed QSO 0957+561 in the wavelength range 2200–3300 Å. We find that the absorption system ($z_{abs} = 1.3911$) near z_{em} is a weak, damped Lyα system with strong Lyα absorption lines seen in both images. However, the H I column densities are different, with the line of sight to image A intersecting a larger column density. The continuum shapes of the two spectra differ in the sense that the flux level of image A increases more slowly toward shorter wavelengths than that of image B. We explain this as the result of differential reddening by dust grains in the damped Lyα absorber. A direct outcome of this explanation is a determination of the dust-to-gas ratio, k, in the damped Lyα system. We derive $k = 0.55 \pm 0.18$ for a simple $1/\lambda$ extinction law and $k = 0.31 \pm 0.10$ for the Galactic extinction curve. For gravitationally lensed systems with damped Lyα absorbers, our method is a powerful tool for determining the values and dispersion of k, and the shapes of extinction curves, especially in the FUV and EUV regions. We compare our results with previous work.

Subject headings: galaxies: ISM — gravitational lensing — quasars: absorption lines — quasars: individual (QSO 0957+561)

1. INTRODUCTION

0957+561 A, B, discovered by Walsh, Carswell, & Weymann (1979; hereafter WCW) are the first examples of multiple images of a gravitationally lensed quasar. This system has an emission redshift of 1.4136 (Weymann et al. 1979), and the separation between the two images is 6″.17 (Roberts et al. 1985). WCW noticed that below 5300 Å the two continua had identical shapes, with image A brighter than B by 0.35 mag at the time of observation. Above 5300 Å, however, the flux from B rose more steeply than that from A, and they were equal at ~6500 Å. They also discovered a low-ionization absorption system at $z_{abs} = 1.390$ and noticed that in the spectrum of image B, the absorption lines appeared to be weaker than the corresponding lines in the spectrum of image A. This latter result was soon confirmed by the MMT spectra of Weymann et al. (1979).

WCW suggested that differential reddening along the two lines of sight might be responsible for the different continuum shape in the two images. In particular, they pointed out that the observed break at 5300 Å corresponded to a wavelength of 2200 Å in the QSO rest frame, and 2200 Å is a well-known resonance feature in interstellar extinction caused by dust grains in the Galaxy. Following this suggestion, Wills & Wills (1980) constructed various dust extinction models to fit the observed continuum shapes. It is obvious that for the dust extinction model to work at optical wavelengths, the extinction must be stronger along the line of sight to image B, since the flux of image B falls faster at shorter optical wavelengths.

Young et al. (1980) found a cluster of galaxies around 0957+561 A, B at redshift ~0.39. They attributed the break in the spectrum of image B to the presence of the brightest member galaxy, G1, superposed on that image. Direct imaging under superb seeing conditions by Stockton (1980) resolved G1. Further observations by Young et al. (1981a) revealed the variability of the two images. The redshift of G1 was redetermined as 0.36. The evidence was convincing, and Wills & Wills (see their Note added in proof) agreed with the G1 galaxy explanation.

We present UV spectra (2200–3300 Å) of 0957+561 A and B obtained with the Faint Object Spectrograph (FOS) on board the *Hubble Space Telescope* (*HST*).[2] In this spectral region we found that the flux level of image A rises more slowly toward the short-wavlength end than does that of image B. We also found that the absorption system ($z_{abs} = 1.3911$) near z_{em} is a weak, damped Lyα system with strong Lyα absorption lines present in both images. However, it is clear that the two H I column densities are different, with the sight line to image A intersecting a large column density.

While the difference in continuum shape in the optical range can be explained by contamination from the lensing galaxy G1, this explanation will not work in the UV. We propose that the difference in the continuum shapes in the UV is due to differential dust grain reddening by the damped Lyα system at $z_{abs} = 1.3911$. In this paper we fit the observations by assuming that dust is mixed with the gas in the damped Lyα clouds. The direct result of this procedure is a determination of the dust-to-gas ratio in the damped Lyα system. We show that by combining optical observations with *HST* spectra the shape of the dust grain extinction curve may also be determined. We compare our results with previous work which determined the dust-to-gas ratio in damped Lyα clouds.

2. OBSERVATIONS AND DATA REDUCTION

On 1995 January 26, UV spectra (2222–3277 Å) of both images of the gravitational lens 0957+561 were obtained with the moderate dispersion G270H grating ($R \approx 1300$) and the Red Digicon of the *Hubble Space Telescope*'s

[1] Based on observations with the NASA/ESA *Hubble Space Telescope*, obtained at STScI, which is operated by AURA, Inc., under NASA contract NAS5-26555.

[2] Program 5683.

COSTAR—corrected Faint Object Spectrograph. The total exposure for image A was 6500 s and that for image B (the South West image with the lensing galaxy about 1″ away) was 6560 s. Since the spectra were sampled at quarter-diode intervals to improve the resolution, the actual exposure times per pixel are one-quarter of these total exposure times. The observations were made through a circular aperture of diameter 0.″43. The target aquisition sequence was designed to center each object to within 0.″04 (0.5 pixel) in order to minimize errors due to flat-field variations. An additional small error in the position of the spectrum on the diode array may arise due to nonrepeatability in the setting of the filter/grating wheel (see below).

The UV absorption lines corresponding to the two optically identified absorption systems (see Young et al. 1981b and references therein) are present in both *HST*/FOS spectra. For the stronger absorption system near z_{em}, Young et al. (1981b) determined an absorption redshift, $z_{abs} = 1.3911$. We adjusted our wavelength scales to set the relatively weak damped Lyα systems in A and B to be at redshift 1.3911. The shifts differ by 0.84 pixels (0.43 Å). Both spectra are plotted in Figure 1.

3. MODEL CALCULATIONS AND RESULTS

3.1. *Continuum Shape and Dust Grain Extinction*

Following Fall & Pei (1989) we write the optical depth due to dust grain extinction as

$$\tau(\lambda) = \tau_B A(\lambda)/A(4400\ \text{Å}) ,$$

where $A(\lambda)$ is the extinction in magnitudes and τ_B is the B band optical depth in the rest frame of an absorber. The dimensionless dust-to-gas ratio, k, is defined as (Fall & Pei 1989)

$$\tau_B = kN_{\text{H I}}/10^{21} ,$$

where $N_{\text{H I}}$ is the H I column density in units of cm^{-2}. For the $A(\lambda)$ extinction curve we consider two models. Model I assumes a simple $A(\lambda) \propto \tau_\lambda \propto 1/\lambda$ law and this leads to

$$\tau(\lambda) = k\left(\frac{N_{\text{H I}}}{10^{21}}\right)\left(\frac{4400\ \text{Å}}{\lambda}\right) \quad \text{(model I)} .$$

In model II we use the mean Galactic extinction law derived by Cardelli, Clayton, & Mathis (1989; hereafter CCM). CCM give the parameterized analytical form of $A(\lambda)/A_V$ for wavelengths $\lambda > 1000$ Å. Since the mean diffuse ISM extinction, $A(\lambda)/A_V$, above 1000 Å is characterized well by the value $R_V = A_V/E(B-V) = 3.1$ (CCM), we adopt this value for Model II. We then have

$$\tau(\lambda) = k\left(\frac{N_{\text{H I}}}{10^{21}}\right)\left[\frac{A(\lambda)}{A_V}\right]\left[\frac{A_V}{A(4400\ \text{Å})}\right] \quad \text{(model II)} .$$

In our case, $\lambda \equiv \lambda_z = \lambda_{obs}/(1 + z_{abs})$, where z_{abs} denotes the absorption redshift of the absorber ($z_{abs} = 1.3911$ in our case). We have extrapolated the CCM expression below 1000 Å and applied it to shorter wavelengths near the Lyman limit ($\lambda = 912$ Å) in our calculations. The Fall & Pei Galactic extinction curve is very similar to our CCM curve, while our simple model I curve falls between the LMC and SMC curves in the wavelength region they used. Thus model I, although very simple, does approximate some realistic dust grain extinction laws.

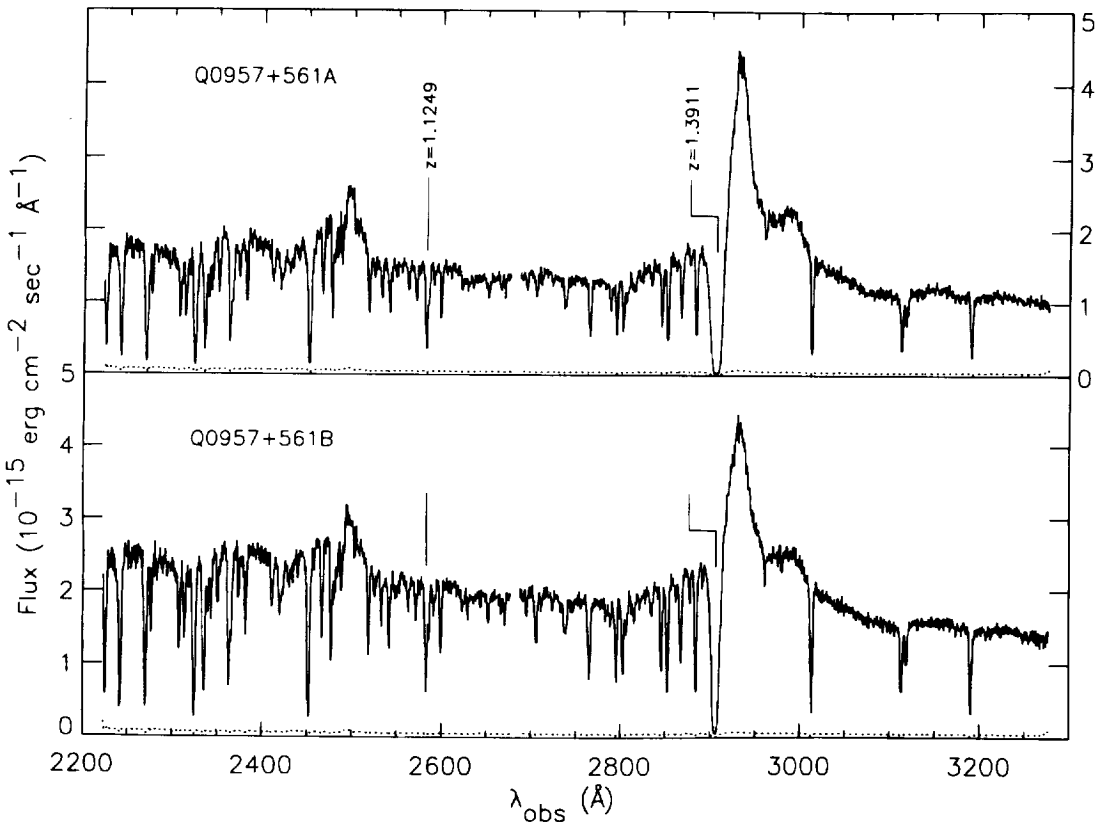

FIG. 1.—The *HST*/FOS spectra of Q0957+561 A, B. Lyα lines in the strong absorption line systems are marked. The upper panel is the spectrum of image A, and the lower panel is the spectrum of image B. A portion of the spectrum near 2680 Å which was contaminated by a noisy diode has been omitted. The 1 σ errors are shown as dotted lines.

The model extinction curves are plotted in Figure 2, normalized to the B band ($\lambda_B = 4400$ Å). The solid line is the CCM curve (model II) and the dashed line is model I. The vertical dashed line represents the short-wavelength limit of the CCM parameterization.

Now let $f^{A}_{\lambda_{obs}}$ and $f^{B}_{\lambda_{obs}}$ be the observed flux from the images A and B, respectively. Let $f^{A}_{\lambda_{obs}}(0)$ and $f^{B}_{\lambda_{obs}}(0)$ be the intrinsic flux before absorption by dust grains in the damped Lyα system. We have

$$\ln\left(\frac{f^{A}_{\lambda_{obs}}}{f^{B}_{\lambda_{obs}}}\right) = \ln\left[\frac{f^{A}_{\lambda_{obs}}(0)}{f^{B}_{\lambda_{obs}}(0)}\right] - \left(1 - \frac{N_B}{N_A}\right)\tau^{A}_{\lambda_z},$$

where N_A and N_B are the H I column densities along the lines of sight to A and B, respectively. For gravitationally lensed images, if there is no time delay, $f^{A}_{\lambda_{obs}}(0)$ and $f^{B}_{\lambda_{obs}}(0)$ have the same shape, and the first term on the right-hand side of the above equation is a constant, independent of λ_{obs}. In reality, however, both time variability and time delay are often observed in gravitationally lensed systems. The above statement is still correct if the variability only changes flux levels and does not change spectral shapes in the wavelength range of interest. We assume this is the case for this calculation.

In Figure 3, $\ln[f^{A}_{\lambda_{obs}}/(0.755 f^{B}_{\lambda_{obs}})]$ is plotted as a function of 4400 Å/λ_{obs}. Since the original spectra of A and B are offset sightly in wavelength, we have interpolated to calculate flux ratios at wavelengths common to both images. The normalization constant, 0.755, is the flux ratio, $f^{A}_{\lambda_{obs}}/f^{B}_{\lambda_{obs}}$, estimated in the wavelength range 3000–3300 Å. In this plot, we excluded the emission lines since they are produced in an extended region much larger than that of continuum source and may be amplified differently in images A and B. We also excluded the regions with strong absorption lines and a short region affected by an intermittent diode. We see clearly in Figure 3 that the flux of image A is weaker at shorter wavelengths relative to image B. This can be easily explained as the result of differential dust grain extinction if the H I column density along the line of sight to A is greater than toward B.

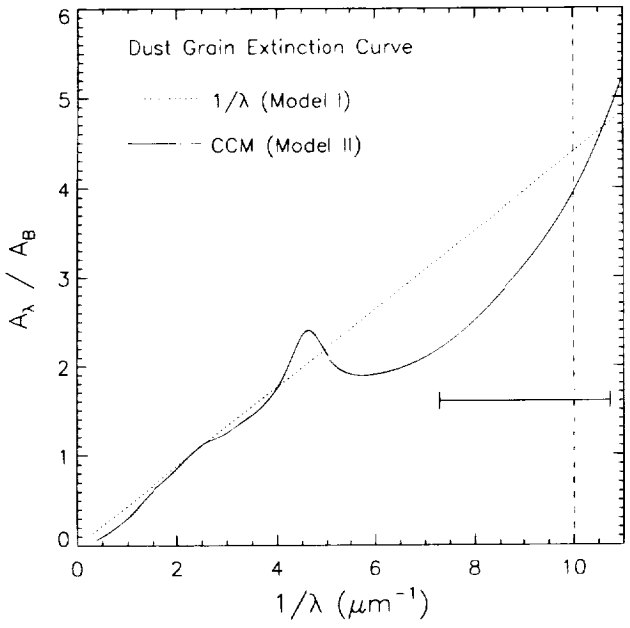

FIG. 2.—The dust grain extinction curves. The solid line is the CCM mean Galactic extinction curve (model II), and the dashed line is the simple $1/\lambda$ extinction law (model I). The vertical dashed line indicates the shortest wavelength in the CCM determination of the mean extinction curve. The horizontal line shows our wavelength coverage in the absorber frame.

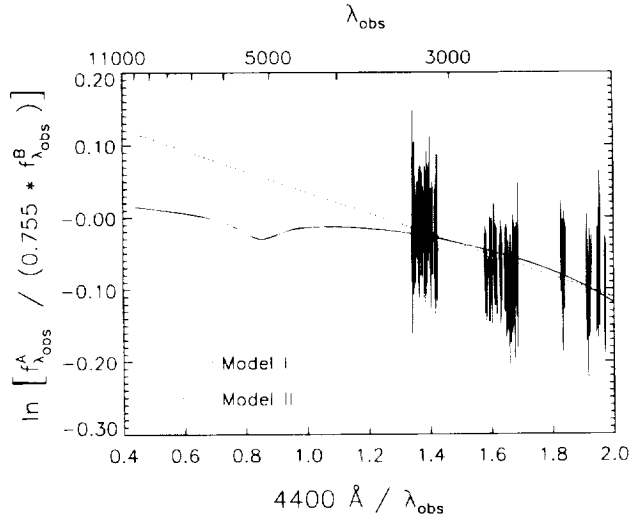

FIG. 3.—Observed flux ratio as a function of 4400 Å/λ_{obs}. The solid line is the model II fit and the dotted line is the model I fit. Notice that the 2200 Å feature in the model II curve is present, but weak. In the optical region, model I and model II predict quite different flux ratios.

3.2. *Column Density Determinations*

The values of the H I column densities, N_A and N_B, can be measured using the damped Lyα lines at $z_{abs} = 1.3911$ present in each spectrum. For each spectrum, an accurate estimate of the unabsorbed Lyα emission-line profile on the blue side is important for determining the column density since it affects the profile determined for the damped Lyα absorption line. We assumed that the intrinsic Lyα emission was symmetric about z_{em}, and reflected the right half of the Lyα emission profile to the left half. The wavelength and height of the peak position of each Lyα emission line were determined by trial and error to provide the best Voigt profile fit to the corresponding damped Lyα absorption. Our results, $N_A = 1.9 \times 10^{20}$ cm^{-2} and $N_B = 8 \times 10^{19}$ cm^{-2}, are plotted as thick solid lines in Figures 4*a* and 4*b*. In Figure 4*a* the dashed line is for $N_A = 2.2 \times 10^{20}$ cm^{-2} and the dotted line is for $N_A = 1.6 \times 10^{20}$ cm^{-2}. In Figure 4*b* the dashed line is for $N_B = 1.0 \times 10^{20}$ cm^{-2} and the dotted line is for $N_B = 6 \times 10^{19}$ cm^{-2}. These values were the extremes of what would be considered reasonable fits. We have used an instrumental resolution FWHM = 2.0 Å in our fits. The results are not sensitive to the resolution because the lines are quite wide. Our column density determinations are both higher than a measurement made in the low-resolution *IUE* spectra of the two images combined, $N = 7 \times 10^{19}$ cm^{-2} ± 30% (Turnshek & Bohlin 1993).

The flux level at the center of the damped Lyα absorption lines does not go to zero in our FOS spectra. This could be either because the scattered light and/or dark background levels were underestimated or because the damped Lyα absorbing cloud is too small to cover the whole quasar emission-line region. Recently Barlow et al. (1996, private communication) found many cases of saturated absorption lines with redshifts near the quasar emission redshift with nonzero residual flux levels at the line centers, even at the very high spectral resolution achieved by the Keck tele-

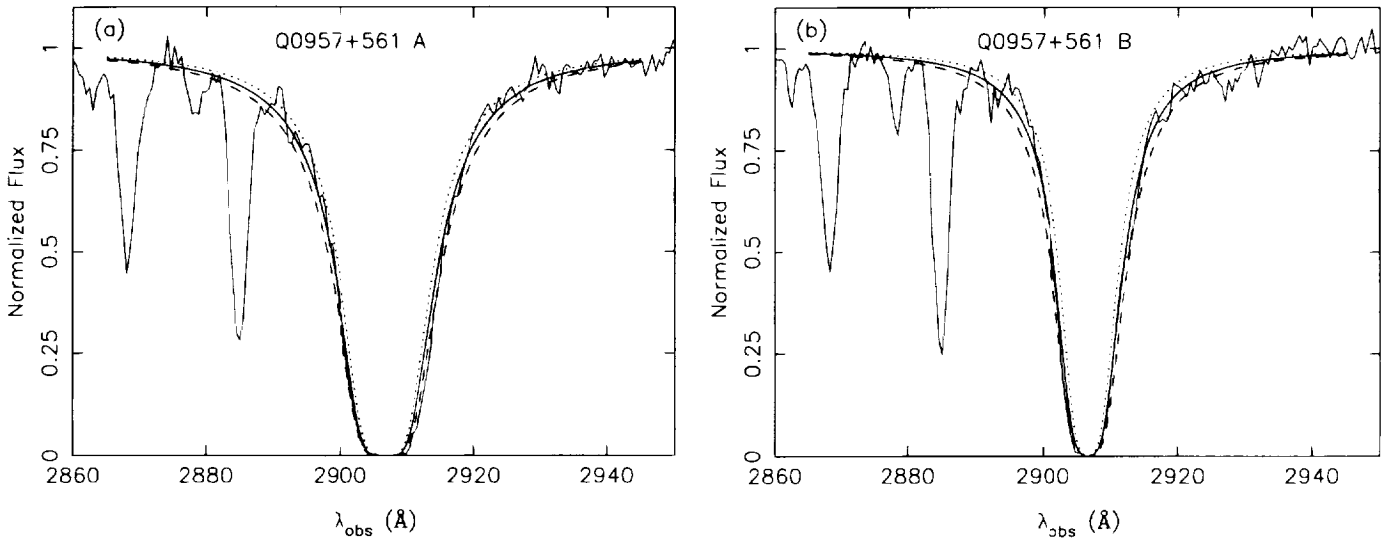

FIG. 4.—(*a*) The fitted Voigt absorption line profiles for the observed (*thin solid line*) damped Lyα absorption in the image A. The thick solid line is our best result $N_{\rm H\,I} = 1.9 \times 10^{20}$ cm^{-2}, the thick dashed line is $N_{\rm H\,I} = 2.2 \times 10^{20}$ cm^{-2}, and the thick dotted line is $N_{\rm H\,I} = 1.6 \times 10^{20}$ cm^{-2}. (*b*) The fitted Voigt absorption line profiles for the observed (*thin solid line*) damped Lyα absorption in the image B. The thick solid line is our best result $N_{\rm H\,I} = 8 \times 10^{19}$ cm^{-2}, the thick dashed line is $N_{\rm H\,I} = 1 \times 10^{20}$ cm^{-2}, and the thick dotted line is $N_{\rm H\,I} = 6 \times 10^{19}$ cm^{-2}.

scope. Incomplete coverage of the quasar emission-line region by absorbing clouds is their favored explanation. Our case is similar to theirs in that $z_{\rm abs} \simeq z_{\rm em}$, but the lines in 0957+561 have much larger column densities. In either case, it would be appropriate to subtract the residual fluxes to force the damped line centers to go to zero level. The residual fluxes subtracted are 3.5×10^{-17} ergs cm^{-2} s^{-1} Å^{-1} in A and 5.8×10^{-17} ergs cm^{-2} s^{-1} Å^{-1} in B. The residual flux level in B sets an upper limit for the contamination by the lensing galaxy G1.

3.3. *Results*

We have used the FIT routine in Press et al. (1992) to fit our model predictions to the observed flux ratio as a function of wavelength. Denoting $a = \ln\{f^{\rm A}_{\lambda_{\rm obs}}(0)/[0.755 f^{\rm B}_{\lambda_{\rm obs}}(0)]\}$ and $b = (1 - N_{\rm B}/N_{\rm A})(kN_{\rm A}/10^{21})(1 + z_{\rm abs})$, we find $a = 0.181 \pm 0.015$ and $b = 0.146 \pm 0.0097$ for model I. For model II we find $a = 0.051 \pm 0.0078$ and $b = 0.080 \pm 0.0062$. These results, plus the measured $N_{\rm A}$ and $N_{\rm B}$, correspond to $k = 0.55$ and $f^{\rm B}_{\lambda_{\rm obs}}(0)/f^{\rm A}_{\lambda_{\rm obs}}(0) = 1.11$ for model I, and $k = 0.31$ and $f^{\rm B}_{\lambda_{\rm obs}}(0)/f^{\rm A}_{\lambda_{\rm obs}}(0) = 1.26$ for model II. The two best fits are plotted in Figure 3 using a dotted line for model I and a solid line for model II.

We have assumed $\sigma(y)$ is a constant, where $y \equiv \ln[f^{\rm A}_{\lambda_{\rm obs}}/(0.755 f^{\rm B}_{\lambda_{\rm obs}})]$, for the FIT routine. $\sigma(y)$ includes the statistical error and the spikes produced by weak absorption lines (we have excluded strong absorption lines) whose profiles in one spectrum are not exactly the same as the corresponding ones in the other spectrum. Judging from Figure 3, our assumption is reasonable. Taking estimates $\sigma(N_{\rm A}) = 3 \times 10^{19}$ cm^{-2} and $\sigma(N_{\rm B}) = 2 \times 10^{19}$ cm^{-2}, our estimations of the error are $\sigma(k) \simeq 0.18$ for model I and $\sigma(k) \simeq 0.10$ for model II. Other possible sources of error which have not been included are uncertainty in the dust grain extinction curve, errors in the continuum levels used to measure the Lyα absorption and possible weak emission lines in our observed wavelength region.

In our determination of the dust-to-gas ratio, we have made several assumptions. We have assumed the environments are similar and k is the same along both lines of sight because of the small separation at the damped Lyα system. (At $z_{\rm abs} = 1.3911$ the separation between the two lines of sight corresponds to a linear size of $0.30\ h_{50}^{-1}$ kpc for $q_0 = 0.5$, and $0.34\ h_{50}^{-1}$ kpc for $q_0 = 0.1$.) From Figure 1 we see that Lyα absorption in the $z_{\rm abs} = 1.1249$ system (Young et al. 1981b) is not very strong, and we can safely neglect its dust grain extinction contribution. The high Galactic latitude ($b \simeq 48°$) and small separation suggests that differential reddening due to the Galaxy is also negligible. Some groups have argued that low-ionization species, such as Zn II and Cr II, can give estimates of both metallicity and dust grain content in damped Lyα clouds (see Meyer & York 1992; Pettini et al. 1995; Wolfe 1995). With the Keck telescope it will be possible to observe these lines in both components and to compare k derived that way with our results. UV monitoring can test our assumption that the intrinsic continuum slopes of the two spectra are the same.

4. COMPARISON WITH PREVIOUS WORK AND DISCUSSION

Since damped Lyα systems are thought to be due to the progenitors of galaxies like our own, they are prime candidates to contain dust grains. A direct indication that dust grains exist in damped Lyα clouds comes from the reddening of background quasars (Fall, Pei, & McMahon 1989; Pei, Fall, & Bechtold 1991; Fall & Pei 1995; hereafter Fall et al.). Fall et al. found that quasars with damped Lyα systems in the foreground tend to appear redder, in a statistical sense, than those without damped Lyα systems in the foreground. Their best determinations for the dust-to-gas ratio in damped Lyα clouds are $k \simeq 0.35^{+0.24}_{-0.09}$ using the Galactic extinction law, $k \simeq 0.09^{+0.06}_{-0.02}$ using the LMC extinction curve, and $k \simeq 0.06^{+0.03}_{-0.01}$ using the SMC extinction curve (Pei et al. 1991). In comparison, the observed dust-to-gas ratios in the Galaxy and the Large and Small Magellanic Clouds are, respectively, $k = 0.79$, $k = 0.19$, and $k = 0.05$ (see Fall & Pei 1989 and references therein).

Before comparing the Fall et al. results with our measurements, we point out that their determinations are made in the wavelength region between the Lyα and C IV emission

lines. It is interesting to see that our model II value, $k = 0.31$, is very similar to their $k = 0.35$ for the Galactic extinction law, given the fact that these values are obtained by two completely different methods. But our model I value of $k = 0.55$ is significantly larger than their LMC and SMC k values. Also our model I k is larger than in model II while Fall et al. get smaller k values for LMC/SMC type extinction than Galactic type extinction. The main reason for the disagreement is that we have a smaller intrinsic flux ratio, $f^{\rm B}_{\lambda_{\rm obs}}(0)/f^{\rm A}_{\lambda_{\rm obs}}(0)$, in model I (1.11) than in model II (1.26), and to produce the observed $f^{\rm B}_{\lambda_{\rm obs}}/f^{\rm A}_{\lambda_{\rm obs}} \simeq 1.32$, we need a larger k for a model I cloud.

Now let us examine why our model I result is so different from the Fall et al. LMC/SMC results. One possibility is that the LMC/SMC type extinction curve is quite different from the simple $1/\lambda$ law at wavelengths shortward of Lyα emission. If this is true, then our model I result will have to be recalculated. At present we know little about the LMC/SMC type extinction curve in the FUV and EUV regions and look forward to future observations that may improve the situation.

Another possible explanation for the discrepancy between our large model I k value and the small k value of Fall et al. is that there is a large dispersion in k. Fall et al. assumed that there is a single k for all damped Lyα absorbers because it is difficult to model the dispersion in k. However, a large dispersion in k is expected for at least two reasons: (i) damped Lyα absorbers are found in various states of chemical evolution; (ii) radial abundance gradients are probably present, and the scatter in impact parameters implies a large spread of k. Boissé (1995) argued that the low dust-to-gas ratio in damped Lyα absorbers may be the result of a selection effect; a smaller mean k value would be favored because QSOs obscured by damped absorbers with large k values may be too faint to be included in spectroscopic samples.

A large dispersion in k seems to be consistent with the observations of metal abundances in damped Lyα systems by Pettini et al. (1995 and references therein). They used Zn as a tracer of metallicity since Zn is relatively undepleted by dust grains, and Zn should also trace Fe, the most widely used indicator of metallicity (Pettini et al. 1995; Wolfe 1995). Pettini et al. found that, while on average the metal abundance in the damped Lyα systems at redshifts $z \simeq 2$–3 is about 1/10 of the solar value, there is a large dispersion, from near solar to less than 10^{-2} of the solar value, in the degree of metal enrichment attained by different damped absorbers at essentially the same epoch. These results are confirmed by the recent observations of Wolfe & Prochaska (1995, private communication) using the HIRES echelle spectrograph on the Keck 10 m telescope. Although it is not known how the metal abundance relates to k directly, it may be that a large dispersion in metallicity means a large dispersion in k. So at the present time we cannot rule out the large model I k value for the 0957+561A, B absorption system. Measurements of Zn and Cr in other damped Lyα systems at redshifts similar to (or lower) than that of 0957+561 imply very low dust-to-gas ratios (Meyer & York 1992; Steidel et al. 1995; Meyer, Lanzetta, & Wolfe 1995). If the value of k we measure here is correct, this implies that there is a considerable range of k at low redshifts as well. A measurement of Zn and Cr in 0957+561 would be an important test.

We should also point out that this damped system redshift is near the quasar emission redshift. It has been suggested that metal absorption systems at $z_{\rm abs} \sim z_{\rm em}$ could be associated with the QSO itself either because they arise in galaxies hosting the QSO or because they are the signature of ejected material (see Petitjean 1995 and the references therein). By studying nine absorption systems in two QSOs, 0424−131 and 0450−131, Petitjean & Bergeron (1994) found that the systems within 10,000 km s^{-1} of the QSO have abundances similar to or even in excess of the solar value. In 0957+561A, B, the difference between $z_{\rm abs}$ and $z_{\rm em}$ corresponds to about 3000 km s^{-1}, and the large model I k value might indicate an enhanced metal abundance near the quasar.

Fall et al. and many others (see the references cited in the Fall et al. papers) have tried but failed to detect the 2200 Å feature of Galactic type dust in damped Lyα absorbers. In Figure 3 we extend the fits for both models into the optical to show this region. It is clear that for $k = 0.31$, observations with exceptionally good S/N would be required to detect the 2200 Å feature of Galactic type dust grains. However, the two models predict quite different flux ratios in the optical region, and it should be possible to select between these models for 0957+561. Observations with the *HST* can exclude any contribution from G1, which currently contaminates the optical spectrum of 0957+561 B, while obtaining the entire optical/UV spectrum simultaneously. If, in addition, observations of A and B are separated by the time delay (see, e.g., Kundić et al. 1995), it will be possible to eliminate errors due to any differences in continuum slopes caused by spectral variability.

Since it may strongly affect our view of the distant universe, dust grain extinction has important cosmological consequences. This topic has been studied by several groups. In these studies dust grains are either associated with intervening galaxies (Ostriker & Heisler 1984; Heisler & Ostriker 1988; Wright 1986, 1990) or attached to quasar absorption-line systems (Fall & Pei 1995; Zuo & Phinney 1993; Ostriker & Vogeley 1990). The advantage of using quasar absorption-line systems is that these are observed in large quantities at high redshifts. The outcome of the obscuration calculations depends critically on the k value used. When more damped Lyα absorbers in gravitationally lensed systems are discovered, the method presented here will become a powerful tool for determining the value and dispersion of k, as well as the shapes of extinction curves, especially in the FUV and EUV regions.

We thank Fred Hamann and Phil Blanco for discussions and Pam Capodicci for assistance with the preparation of the manuscript. This work has been supported by NASA NAS5-29293 and NAG5-1630.

REFERENCES

Barlow, T. 1996, private communication
Boissé, P. 1995, in QSO Absorption Lines, ed. G. Meylan (Berlin: Springer), 35
Cardelli, J. A., Clayton, G. C., & Mathis, J. S. 1989, ApJ, 345, 245 (CCM)
Fall, S. M., & Pei, Y. 1989, ApJ, 337, 7
Fall, S. M., & Pei, Y. 1995, in QSO Absorption Lines, ed. G. Meylan (Berlin: Springer), 24
Fall, S. M., Pei, Y., & McMahon, R. G. 1989, ApJ, 341, L5
Heisler, J., & Ostriker, J. P. 1988, ApJ, 332, 543
Kundić, T., et al. 1995, ApJ, 455, L5

Meyer, D. M., Lanzetta, K. M., & Wolfe, A. M. 1995, ApJ, 451, L13
Meyer, D. M., & York, D. 1992, ApJ, 399, L121
Ostriker, J. P., & Heisler, J. 1984, ApJ, 278, 1
Ostriker, J. P., & Vogeley, M. S. 1990, ApJ, 364, 405
Pei, Y., Fall, S. M., & Bechtold, J. 1991, ApJ, 378, 6
Petitjean, P. 1995, in QSO Absorption Lines, ed. G. Meylan (Berlin: Springer), 61
Petitjean, P., & Bergeron, J. 1994, A&A, 283, 759
Pettini, M., King, D. L., Smith, L. J., & Hunstead, R. W. 1995, in QSO Absorption Lines, ed. G. Meylan (Berlin: Springer), 71
Press, W. H., Teukolsky, S. A., Vetterling, W. T., & Flannery, B. P. 1992, Numerical Recipes in C (Cambridge: Cambridge Univ. Press)
Roberts, D. H., Greenfield, P. E., Hewitt, J. N., Burke, B. F., & Dupree, A. K. 1985, ApJ, 293, 356
Steidel, C. C., Bowen, D. V., Blades, J. C., & Dickinson, M. 1995, ApJ, 440, L45
Stockton, A. 1980, ApJ, 242, L141
Turnshek, D. T., & Bohlin, R. C. 1993, ApJ, 407, 60
Walsh, D., Carswell, R. F., & Weyman, R. J. 1979, Nature, 279, 381
Weymann, R. J., Chaffee, F. H., Davis, M., Carleton, N. P., Walsh, D., & Carswell, R. F. 1979, ApJ, 233, L43
Wills, B. J., & Wills, D. 1980, ApJ, 238, 1
Wolfe, A. 1995, in QSO Absorption Lines, ed. G. Meylan (Berlin: Springer), 13
Wolfe, A., & Prochaska, J. 1995, private communication
Wright, E. L. 1986, ApJ, 311, 156
———. 1990, ApJ, 353, 411
Young, P., Gunn, J. E., Kristian, J., Oke, J. B., & Westphal, J. A. 1980, ApJ, 241, 507
———. 1981a, ApJ, 244, 736
Young, P., Sargent, W. L. W., Boksenberg, A., & Oke, J. B. 1981b, ApJ, 249, 415
Zuo, L., & Phinney, E. S. 1993, ApJ, 418, 28